



ELSEVIER

NeuroImage

www.elsevier.com/locate/ynimg  
NeuroImage xx (2007) xxx–xxx

## Automated deformation analysis in the YAC128 Huntington disease mouse model

Jason P. Lerch,<sup>a,\*</sup> Jeffrey B. Carroll,<sup>c,1</sup> Shoshana Spring,<sup>a</sup> Lisa N. Bertram,<sup>b</sup> Claudia Schwab,<sup>b</sup> Michael R. Hayden,<sup>b</sup> and R. Mark Henkelman<sup>a</sup>

<sup>a</sup>Mouse Imaging Centre (MICE), Hospital for Sick Children, 555 University Ave., Toronto, ON, Canada M5G 1X8

<sup>b</sup>Centre for Molecular Medicine and Therapeutics, Child and Family Research Institute, Department of Medical Genetics, University of British Columbia, Vancouver, British Columbia, Canada

<sup>c</sup>Centre for Molecular Medicine and Therapeutics, Child and Family Research Institute, Department of Neuroscience, University of British Columbia, Vancouver, British Columbia, Canada

Received 30 May 2007; revised 23 July 2007; accepted 17 August 2007

The YAC128 mouse recapitulates many of the clinical features of Huntington disease (HD), including selective neuropathology with neuronal loss. Here we investigate whether differences in neuroanatomy could be detected using high-resolution magnetic resonance (MR) imaging earlier than the previously defined 9-month age of onset of striatal neuropathology. The striatum is significantly decreased in volume (3.4%,  $p < 0.02$ ) at 8 months of age. A subset of the brains was also analyzed using stereology, and the MR measures were found to be more robust at separating the two groups of mice. Striatal degeneration was found to be asymmetric, with the dorsal and lateral aspects of the striatum being most affected. Non-striatal changes in neuroanatomy were also investigated, revealing regions of expansion as well as atrophy. Our findings suggest that MR imaging can be used to detect and monitor subtle anatomical differences throughout the whole brain and at early time points in the YAC128 mouse-model of HD.

© 2007 Elsevier Inc. All rights reserved.

**Keywords:** Huntington disease; MRI; Neurodegeneration; Striatum; Mouse models; Neuroanatomy

### Introduction

Huntington disease (HD) is a neurodegenerative disorder characterized by motor dysfunction, psychiatric disturbances and cognitive impairment that is caused by a CAG trinucleotide expansion in the *HD* gene on chromosome 4 (Huntington's Collaborative Research, 1993). HD is classically associated with reduction in volume and neuronal loss initially primarily localized

to the striatum (Vonsattel et al., 1985), but widespread brain atrophy has been described in early to mid-stage HD using magnetic resonance (MR) techniques (Rosas et al., 2003). MR techniques have also been used to monitor pre-symptomatic HD mutation carriers, demonstrating a strong correlation between caudate and putamen volumes and disease onset (Aylward et al., 2004). Longitudinal MR imaging of HD patients has been proposed as a biomarker of disease progression (Aylward, 2007).

We have generated the YAC128 mouse model of HD that expresses the entire human *huntingtin* (*htt*) gene with 120 CAG repeats (Slow et al., 2003). This mouse model recapitulates many features of human HD including progressive motor and cognitive deficits, striatal and cortical atrophy with relative sparing of the hippocampus and cerebellum. These animals demonstrate low inter-animal variability (Slow et al., 2003; Van Raamsdonk et al., 2005a,d). As in human HD, the phenotype of the YAC128 mouse is progressive, with cognitive deficits detectable as early as 2 months, followed by motor deficits and specific striatal and cortical atrophy (Slow et al., 2003; Van Raamsdonk et al., 2005d). Striatal atrophy in YAC128 is associated with a decrease in neuronal count, and striatal neuronal loss at later time points correlates strongly with earlier motor deficits (Slow et al., 2003).

A recent investigation into the neuropathology of the YAC128 mouse using stereological methods demonstrated volume loss in specific regions of the brain (Van Raamsdonk et al., 2005a). The striatum, globus pallidus and cortex show decreased volume at 12 months of age, while no change in the hippocampus or cerebellum could be detected at this time. In order to further characterize this model, we undertook the current study using MRI techniques, which have been increasingly used for the phenotyping of mouse models (Nieman et al., 2005; Kovacevic et al., 2005). MR has the advantages of providing whole brain coverage and allowing investigation of genotype related changes throughout the cerebrum without having to define prior regions of interest. Recent studies have found fine-grained differences between three separate inbred

\* Corresponding author. Fax: +1 416 813 2208.

E-mail address: jason@sickkids.ca (J.P. Lerch).

<sup>1</sup> These authors contributed equally.

Available online on ScienceDirect (www.sciencedirect.com).

mouse strains (Chen et al., 2006), shown atrophy in the experimental autoimmune encephalomyelitis model of multiple sclerosis (MacKenzie-Graham et al., 2006), and characterized anatomical deficiencies in cerebellar-deficient folia (cdf) mutation mice (Bock et al., 2006). The cdf study mentioned above was able to corroborate the MR-detected changes with histology (Bock et al., 2006), providing evidence for the validity of MR-based techniques of assessing neuroanatomical phenotypes.

MRI is furthermore a modality that can span mouse models and human clinical studies. Several investigations using MRI in human populations with Huntington disease have found decreases in striatal and white matter volumes (Paulsen et al., 2006; Aylward et al., 1998), decreases in cortical thickness and volume in later stages of the disease (Rosas et al., 2002) along with some indications of increased cortical volume in pre-clinical HD (Paulsen et al., 2006). Replication of these human imaging results in a mouse model of HD would provide further evidence of the validity of the mouse model.

The YAC128 mouse represents an important model to test the therapeutic efficiency of interventions in HD. Longitudinal *in vivo* imaging of live YAC128 mice would allow a complete natural history of neuropathology to be developed during clinical trials, increasing the power to detect therapeutic efficacy over a single measurement of neuropathology. The goal of this study was thus to use high-resolution MRI to further characterize YAC128 mice (Slow et al., 2003; Van Raamsdonk et al., 2005d), compare MR- and stereology-based striatal volumes, and to provide proof of principle for future longitudinal imaging studies in YAC128 mice undergoing therapeutic trials.

## Materials and methods

### Sample preparation

Eight-month-old FVB/N (Charles River, Wilmington, MA) and YAC128 transgenic HD model mice maintained on a FVB/N background were anesthetized with a combination of Ketamine (100 mg/kg) and Rompun (20 mg/kg) via intraperitoneal injection. A previously described sample preparation protocol for scanning was used with slight modifications (Tyszka et al., 2006). Thoracic cavities were opened and animals were perfused through the left ventricle with 30 mL of phosphate-buffered saline (PBS) (pH 7.4) at room temperature (25 °C). This was followed by infusion with 30 mL of iced 4% paraformaldehyde (PFA) in PBS. Following perfusion, the heads were removed along with the skin, lower jaw, ears and the cartilaginous nose tip. The remaining skull structures containing the brain were allowed to postfix in 4% PFA at 4 °C for 12 h. Following an incubation period of 5 days in PBS and 0.01% sodium azide at 15 °C, the skulls were transferred to a PBS and 2 mM ProHance® (Bracco Diagnostics Inc., Princeton, NJ) solution for at least 7 days at 15 °C. MR imaging occurred 12 to 21 days post-mortem. All the animal experiments were approved by the animal ethics committee of the University of British Columbia. Nine brains each in the wild-type and YAC128 mouse groups were imaged.

### MR acquisition

A multi-channel 7.0 T MRI scanner (Varian Inc., Palo Alto, CA) with a 6-cm inner bore diameter insert gradient set was used to acquire anatomical images of brains within skulls. Prior to imaging,

the samples were removed from the contrast agent solution, blotted and placed into 13-mm-diameter plastic tubes filled with a proton-free susceptibility-matching fluid (Fluorinert FC-77, 3M Corp., St. Paul, MN). Three custom-built, 14-mm-diameter solenoid coils with a length of 18.3 cm and over wound ends were used to image three brains in parallel. Parameters used in the scans were optimized for grey/white matter contrast: a T2-weighted, 3D fast spin-echo sequence, with TR/TE=325/32 ms, four averages, field-of-view  $12 \times 12 \times 25$  mm and matrix size=432×432×780 giving an image with 32  $\mu$ m isotropic voxels. Total imaging time was 11.3 h. Geometric distortion due to position of the three coils inside the magnet was corrected using an MR phantom.

### Atlas creation

An unbiased model independent atlas of the 18 MR scans was created through the following procedure (Kovacevic et al., 2005; Chen et al., 2006). All scans were linearly (3 rotations, 3 translations) registered towards a pre-existing atlas. All possible pairwise 12-parameter registrations (3 scales, 3 shears, 3 rotations, 3 translations) were then computed, and an average transform created for each mouse. All scans were then averaged to create the first population atlas, representing the average anatomy of the study sample after accounting for overall brain-size differences. An iterative 6-generation multi-scale non-linear alignment procedure was then begun, initially registering each mouse towards the 12 parameter registration atlas, and subsequently towards the atlas of the previous non-linear generation. All registrations were performed using the mni\_autoreg tools (Collins et al., 1994; Collins et al., 1995), which use an elastic registration algorithm (see Table 1 for the exact deformation schedule). The end-result is to have all 18 scans deformed into exact alignment with each other in an unbiased fashion. This allows for the analysis of the deformations needed to take each mouse's anatomy into this final atlas space, the goal being to model how the deformation fields relate to genotype.

Table 1  
Listing of the non-linear deformation schedule

Step	Grid resolution ( $\mu$ m)	Iterations	Gaussian FWHM/( $\mu$ m) feature
Step 1.1	700	60	300 intensity blur
Step 1.2	700	60	300 gradient magnitude
Step 2.1	600	15	200 intensity blur
Step 2.2	600	15	200 gradient magnitude
Step 3.1	500	15	200 intensity blur
Step 3.2	500	15	200 gradient magnitude
Step 4.1	400	15	200 intensity blur
Step 4.2	400	15	200 gradient magnitude
Step 5.1	300	15	200 intensity blur
Step 5.2	300	15	200 gradient magnitude
Step 6.1	60	15	100 intensity blur
Step 6.2	60	15	100 gradient magnitude

Listing of the non-linear deformation schedule used. 6 non-linear generation were created, each generation using two fits, one to the blurred image intensities followed by a fit to the magnitude of the gradient of the blur. A 3D simplex optimization for local deformations was used, with the stiffness, weight, and similarity values set to 0.98, 0.8, and 0.8, respectively. The highly accurate ability of this algorithm to align neuroanatomical features in the mouse brain is shown in Spring et al. (2007).

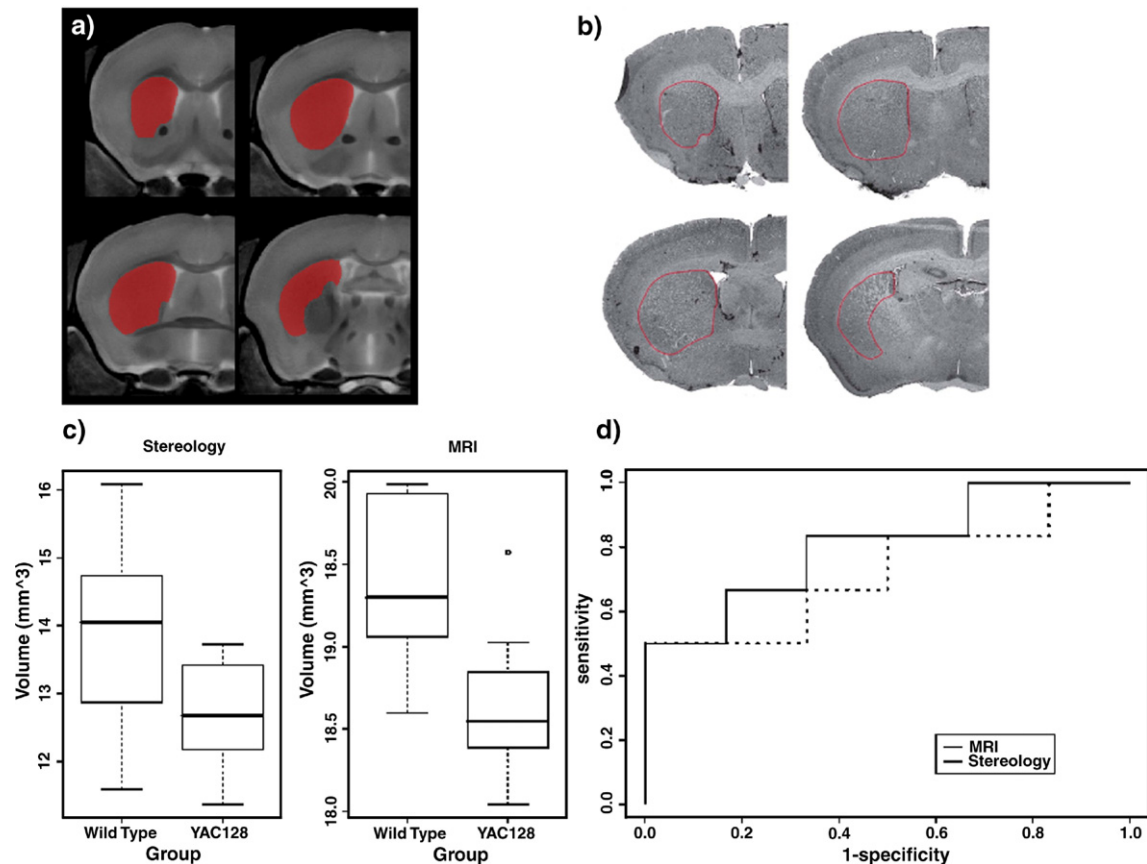


Fig. 1. (a) An example of the atlas segmentation of the striata from MRI, and (b) four coronal Cresyl violet-stained slices which show the delineation used to derive striatal volumes using stereology. (c) Two box and whiskers plots showing differences in estimated striatal volume from 12 brains which underwent both stereology and MR imaging. Extra variance in the stereology estimates explains why no significant differences between groups ( $p < 0.07$ ) were found using stereology, whereas the MR volume estimates were able to detect significant change ( $p < 0.03$ ). Part (d) shows an ROC curve comparing the accuracy and specificity of striatal volumes from MRI and stereology. The area under the curve was 0.81 for MR volumes and 0.72 for the stereology measures. The differences in absolute volumes between the two measures are likely due to tissue shrinkage during specimen preparation for histology.

### Striatal volumes

The striatum was segmented on the final atlas resulting from the MR image registration process. The transforms from each mouse towards the final atlas were then inverted and the segmented striatum back propagated to each MRI. The volume of the striatum was then analyzed for group differences using a one-tailed  $t$  test (Fig. 1a).

### Stereology

After MR acquisition, the fixed brains were removed from the skull and transferred to 30% sucrose in phosphate-buffered saline (pH 7.4, 0.1 M) for 2 days. Immediately prior to sectioning, brains were frozen on dry ice. Serial coronal sections (25  $\mu$ m) were cut on a cryostat microtome (HM 500 M, Microm Int. GmbH, Walldorf, Germany). Every eighth section was mounted on glass slides and stained with Cresyl violet. The area of the striatum was traced using Stereoinvestigator software (Microbrightfield) in each section between the anterior start of the crossing of the corpus callosum and the anterior start of the hippocampus (Fig. 1b). Striatal volumes were then calculated with Stereoinvestigator software. Due to some desiccation of tissue, only 12 brains scanned were of sufficient quality for stereological analysis. MR and

histology measures were compared using receiver operating characteristic (ROC) curves.

### Striatal shape differences

The goal of the striatal shape analysis is to describe the movement inwards and outwards for each point on the surface of the striatum, and thus provides an elegant way of understanding how the striatum is changing in shape and size. This is accomplished by establishing the boundary of the striatum as well as lines perpendicular to this boundary. By looking at the registration needed to get each mouse into the final atlas space described above combined with these perpendicular lines one can assess, at each point of the striatum's boundary, whether the boundary at that location moved inwards or outwards.

The exact procedure was the following (see Fig. 2): A surface representation of the segmented striatum of the final non-linear atlas was generated using the marching cubes algorithm, and subsequently simplified to contain 18,000 polygons using AMIRA (Mercury Computer Systems Inc.). The dot product of the surface normal (a unit vector describing the direction perpendicular to the surface) of the atlas striatum with the inverted deformation field from each mouse was calculated. The dot products were then

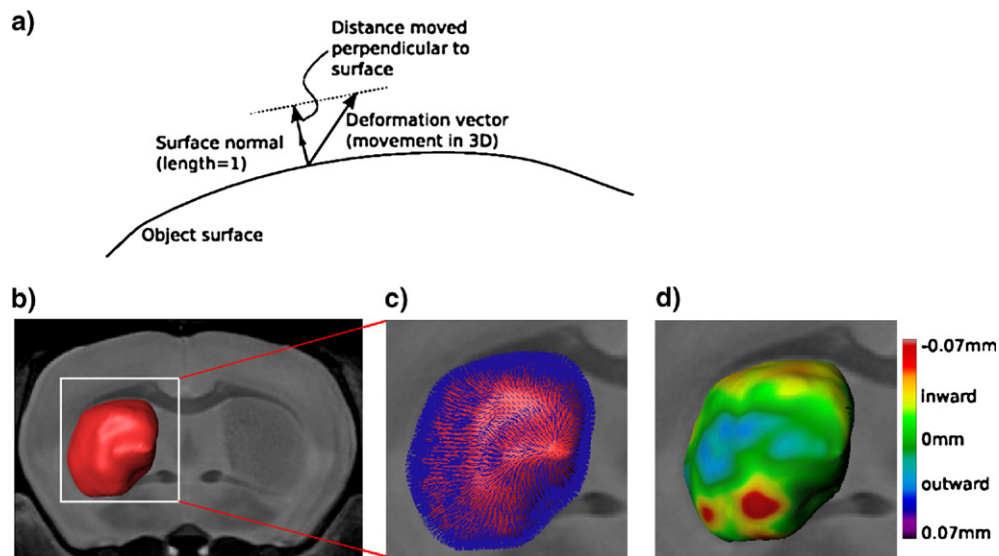


Fig. 2. Growth and shrinkage of the striatum were studied by measuring the movement along the surface normal at each point of the striatum. This metric is shown in panel a) the surface normal is the direction perpendicular to the surface with a normalized length of 1. The deformation vectors (3-dimensional vectors where the magnitude corresponds to distance moved along vector) computed by the registration algorithm, then have their dot-product computed with the surface normal, giving the distance of the surface moved inwards (if the value is negative) or outwards (if positive) along the surface normal. The surface of the striatum is shown in red in part (b). The dot product of the surface normals, shown as small blue arrows on the surface representation in panel c), with the deformation vectors of the inverse of the final non-linear transform, shown coloured by magnitude in panel d), was then taken for each subject.

blurred along the surface using a diffusion smoothing kernel (Chung et al., 2003) with a full-width at half maximum (FWHM) of 300  $\mu\text{m}$ . The blurred dot products were analyzed for group differences using a *t* test.

#### Global shape analysis

The inverted deformation fields were then blurred with a 500- $\mu\text{m}$  Gaussian kernel and analyzed for shape difference across the entire brain. The Jacobian determinant of the deformation fields, which provides an index of voxel expansion and contraction, was computed at every voxel (Chung et al., 2001). The result is a map of *t*-statistics with 16 degrees of freedom.

#### Multiple comparisons

The statistical analysis described above result in millions of separate statistical tests. In order to account for an inflated type I error, the False Discovery Rate (FDR) technique was applied (Genovese et al., 2002) with a 0.1 FDR threshold. The threshold corresponded to an uncorrected *p* value of 0.0043,  $t_{(16)} > 2.99$ . The interpretation of these results is that, on average, 10% of the voxels shown as significant will be false positives.

## Results

#### Striatal volumes and shape

The striata of the YAC128 mice were reduced in size by 3.4% when compared to wild-type mice ( $p=0.02$ ) at 8 months of age. Mean volume was  $19.9 \pm 0.2 \text{ mm}^3$  for the wild-types and  $19.2 \pm 0.3 \text{ mm}^3$  for the YAC128 mice. There was significant loss of tissue (see Fig. 3) in the superior and lateral aspects of the striatum, whereas the medial and inferior aspects appeared spared. The trend towards

loss of tissue was seen bilaterally, but was stronger for the right striatum. The maximum detected inwards movement was 71  $\mu\text{m}$ .

#### Comparison between MR and stereology

Stereology-based striatal volumes were available for 12 of the 18 brain in this study. Using these 12 samples, the striatal volume was reduced by 8.5%, though the effect was not significant ( $p < 0.07$ ). The MR-based striatal volumes of the same 12 brains showed a reduction of 3.3% in the YAC128 mice, an effect that was significant ( $p < 0.03$ ). MR- and stereology-based volumes were further compared using an ROC curve (see Fig. 1d), with the MR volumes showing an area under the curve of 0.81, stereology 0.72. MR and stereology measures were, not surprisingly, strongly correlated ( $r=0.68$ ,  $p < 0.01$ ).

#### Whole brain analysis

At 8 months of age, global brain size was decreased by 2% in the YAC128 mice compared to wild-type, although this did not reach statistical significance ( $p < 0.24$ ). When regional changes were examined, YAC128 mice had significantly contracted voxels (as measured using Jacobian determinants) in the striatum, the corpus callosum, olfactory bulb, thalamus, paraflocculus, and anterior commissure when compared to wild-type mice. Regions of the brain were also found to be significantly larger in YAC128 animals in comparison to wild-type animals, including the primary sensorimotor cortex, primary motor cortex, fimbria, and parts of the cerebellum (Fig. 4, Table 2).

## Discussion

The YAC128 model is a powerful tool for therapeutic trials in HD (Van Raamsdonk et al., 2006; Van Raamsdonk et al., 2005b,c), and

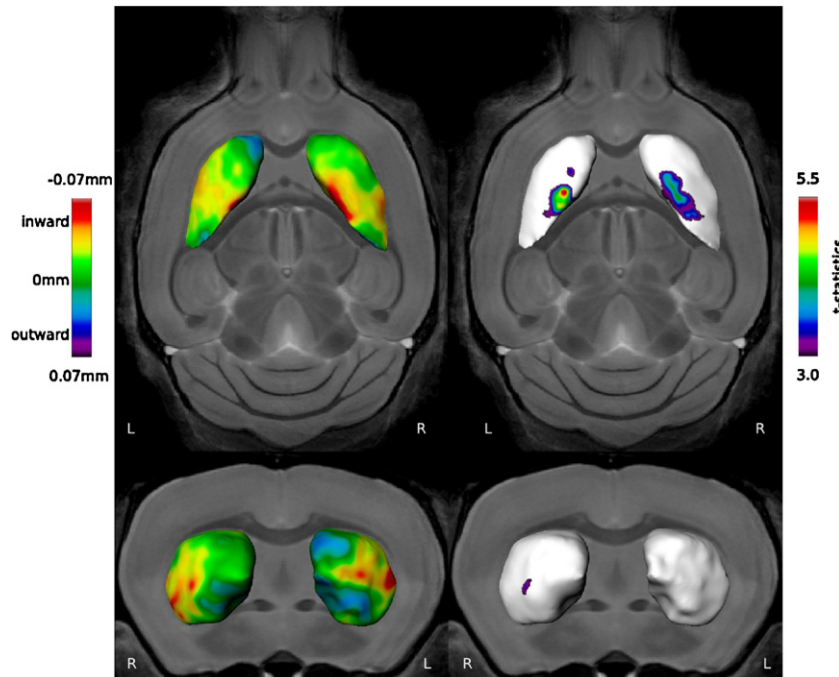


Fig. 3. The striatum is reduced in size in the YAC128 mice compared to wild-type controls. The left images show the group differences in surface position; the right images show the  $t$ -statistics thresholded at a false discovery rate of 0.1. The differences are bilateral though more extensive in the right hemisphere, showing an indentation in superior and lateral aspects of the striatum, with the inferior and medial boundaries spared.

its specific neuropathology is a reliable and quantitative primary endpoint for these trials. MRI has the potential to facilitate longitudinal analysis of neuropathology *in vivo* because live mice can be scanned on different occasions (Bock et al., 2006), allowing a natural history of neuropathology rather than a single, terminal, time point. The present study has provided proof of principle of the power of MR imaging of YAC128 mice, not only by discerning early decreases in striatal volume in a more sensitive fashion than the usually employed stereological methods, but also revealing novel features of the neuropathology in HD. The YAC128 mice have striatal atrophy which is asymmetric within the striatum (Fig. 3). Additionally, unbiased whole brain analysis of MR images reveals a complete picture of neuroanatomical changes in the YAC128 mice, including regions of expansion as well as atrophy (Fig. 4; Table 2).

We have previously reported a 15% decrease in striatal volume in the YAC128 mice at 9 months of age using stereological methods (Slow et al., 2003). YAC128 mice analyzed at 6 months using the same techniques demonstrated no striatal volume loss when compared to wild-type littermates (Slow et al., 2003). Similarly, YAC128 mice have normal brain weights at 6 months of age, but a 5% decrease in brain weight is detectable by 9 months (Slow et al., 2003). The earliest significant cortical atrophy in YAC128 animals was detected at 12 months (Slow et al., 2003). Behavioral differences, such as hypokinesia and impaired rotorod learning, can be detected as early as 2 months of age (Slow et al., 2003; Van Raamsdonk et al., 2005d). Prior investigations of neuropathology in YAC128 mice were conducted using stereological techniques, which require manual delineation of anatomical areas. In this manner, many brain regions have been analyzed including the striatum, cortex (Slow et al., 2003), hippocampus, globus pallidus and cerebellum (Van Raamsdonk et al., 2005a), a strength of MRI – fully 3D whole brain coverage – allows a more

complete view of the neuroanatomical changes in the YAC128 mice.

Significant differences between YAC128 and wild-type mouse brains are detectable by MRI at 8 months of age, 1 month earlier than previously described losses ascertained by stereology (Slow et al., 2003). MR assessment of the striatum showed a significant ( $p < 0.02$ ) 3.4% reduction in volume at 8 months of age. We directly compared stereology to MR data as part of this study. Stereology-based estimates of the striatal volumes in 12 brains in this data (Fig. 1) were unable to detect a significant difference ( $p < 0.16$ ) between the YAC128 mice and wild-type controls at 8 months. This was primarily due to an increase in variance with stereology measures relative to MR. This clearly demonstrates the superiority of MR over stereology in this analysis, also shown by comparing the ROC curves of the two methods, with a greater area under the curve (0.81) for MR volumes vs. stereology (0.72). The fully automated nature of computing striatal volumes based on automated registration techniques is a further advantage over stereology.

Numerous other novel features of the neuropathology in YAC128 mice became evident using MR techniques. Asymmetry in striatal neurodegeneration in the YAC128 mice was observed using MR techniques, the striatum (Fig. 3) showed particular inwards bending in its superior and lateral aspects while the medial wall was spared. This finding is in agreement with previous investigations of YAC HD mice that have shown more pronounced neurodegenerative changes in the lateral aspect of the striatum (Hodgson et al., 1999). Similarly, striatal degeneration is asymmetrical in human HD patients (Vonsattel et al., 1985). The early anterior/lateral degeneration observed in the YAC128 striatum at 8 months implies a different axis of atrophy when compared to the medial to lateral, posterior to anterior and dorsal to ventral degeneration seen in human HD (Vonsattel et al., 1985). These

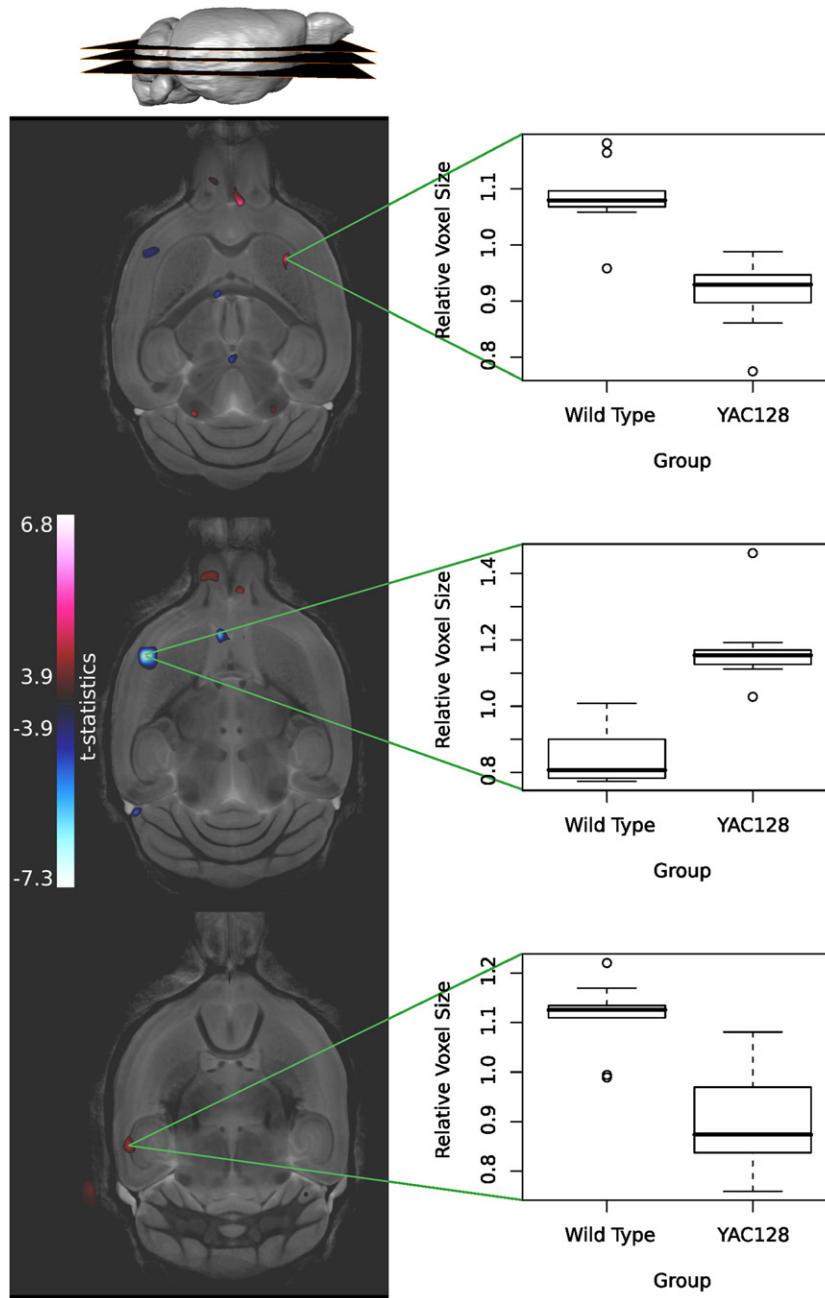


Fig. 4. The per-voxel results of tests of the Jacobian maps (tissue compression/expansion). Three of the most significant voxels are illustrated with a box-and-whiskers plot – one showing the voxel expansion in the left cortex, the others showing the voxel compression in the right striatum as well as the corpus callosum. All coloured voxels are significant with a false discovery rate of 0.1. The top left brain indicates the location of the three slices.

differences in direction could be due to anatomical differences between the basal ganglia of rodents and primates.

Asymmetry is also observed between the left and right striatum, with more significant atrophy in the right than the left striatum in the YAC128 mice at 8 months (Fig. 3). Again, studies in human HD have demonstrated asymmetry of striatal degeneration, similar to that seen in the YAC128 mice (Rosas et al., 2001; Kipps et al., 2005). In humans, the lateralization of striatal neuropathology correlates with increased lactate levels (Jenkins et al., 1998), which lends support to excitotoxicity as a cause of cell death in HD.

We have previously described the correlation between tissue-specific nuclear localization of N-terminal fragments of mutant *huntingtin* and neurodegeneration in the YAC128 mice (Van Raamsdonk et al., 2005a). Selective nuclear localization of mutant *htt* can be detected at 2 months of age, and is associated with neuron loss and tissue atrophy later in the life span of YAC128 animals (Van Raamsdonk et al., 2005a). The accumulation of nuclear fragments of mutant *huntingtin* in the striatum has a lateral to medial gradient, in a manner analogous to the gradient of neurodegenerative changes in YAC HD mice (Hodgson et al., 1999). Shape analysis using 3D MRI reveals that the earliest degeneration in the striatum of the YAC128

Table 2  
Listing of the significant group differences using Jacobian determinants

YAC128<Wild type		YAC128>Wild type	
Location of peak	T-statistics	Location of peak	T-statistics
Left inferior colliculus	5.5	Right sensorimotor cortex	−7.3
Right striatum	5.5	Right cerebellum	−6.6
Right thalamus	5.2	Left lateral septum	−6.2
Left corpus callosum	5.1	Left cerebellum	−5.7
Right frontal cortex/ Olfactory bulb	5.1	Left fimbria	−5.0
Left cerebral peduncle	4.9	Left entorhinal cortex	−4.7
Right paraflocculus	4.3	Left superior colliculus	−4.6
Right anterior commissure	4.2	Left frontal cortex	−4.5

A listing of the significant group differences using Jacobian determinants. Positive *t*-values indicate relative shrinkage in the YAC128 mice, negative values indicate relative growth. The values in each row correspond to a single voxel located within the anatomical region indicated, and thus does not necessarily reflect overall size changes of that structure.

mice is in the superior and lateral aspects (Fig. 3). The correlation between nuclear localization of mutant *huntingtin* and early atrophy supports the importance of nuclear localization of mutant *huntingtin* as a marker for the development of neuropathology in HD.

While most of the focus on neuropathological changes in HD has been on degenerative changes, intriguing MR studies of human HD suggest that the gray matter of the cortex can actually increase in volume pre-clinically before atrophy during the course of the disease (Paulsen et al., 2006; Rosas et al., 2002). Additionally, studies have revealed increased proliferation and neurogenesis in the subependymal layer adjacent to the caudate nucleus in human HD brain (Curtis et al., 2003, Curtis et al., 2005). Increased proliferation in the subventricular zone and new striatal neurons are also observed after quinolinic acid injection into the rat striatum (Tattersfield et al., 2004). The cerebral cortices of the YAC128 mice had areas of increased as well as decreased volume at 8 months (Table 2). The pattern of shrinkage and growth seen in the 8-month-old YAC128 mice (Fig. 4, Table 2) might thus be indicative of a similar pattern as that seen in humans, with atrophy starting in the frontal and secondary motor cortices, while the primary sensorimotor and primary motor cortices are still relatively larger than in wild-type mice. Understanding the dynamic nature of cortical neurodegeneration in the YAC128 mice could provide a powerful tool for understanding which portions of the cortex are most affected by HD. This knowledge could inform cognitive and psychological testing in human HD patients, allowing finer neuropsychological correlates to be found to track pathological changes in human trials.

The power of the analyses used in this study is directly dependent on the natural variability in mouse neuroanatomy, detection sensitivity of the MR acquisition, and accuracy of the deformation-based analysis pipeline. A previous study of gender differences in 20 male and 20 female C57BL/6 mice has shown that the analysis algorithm and data acquisition methodology herein can align small as well as large neuroanatomical features with considerable accuracy (Spring et al., 2007). The standard deviation of the deformation magnitudes (SDDM; a measure of positional variance at each voxel (Kovacevic et al., 2005)) in that dataset was 102  $\mu$ m, providing an estimate of the natural variability of neuroanatomy. The resolution obtained in this study was, however, not enough to resolve cellular differences or

changes in extremely small structures that do not resolve at 32  $\mu$ m voxels; these changes would thus have been missed.

The use of MR images and advanced image processing has allowed for a detailed examination of anatomical differences between YAC128 mice and wild-type mice. We have shown the efficacy of MR in demonstrating differences *in vitro* at a single time point. Future longitudinal *in vivo* MRI will allow us to investigate disease progression over the life span of a single mouse, which will greatly facilitate future treatment trials in the YAC128 mice. These *in vivo* datasets will necessarily suffer from a drop in resolution since living mice cannot be kept under anesthesia for longer than 3 h; we expect that this will be partially compensated by the addition of longitudinal data and the use of mixed-effects statistical models. The approach used in this manuscript will provide significant benefit for trials of long duration that rely upon neuropathological improvement as a primary endpoint.

## Acknowledgments

This work was supported by grants from the Michael Smith Foundation for Health Research, the Canadian Institutes of Health Research, the Huntington's Disease Society of America and the High Q Foundation. J.P.L. is supported by the Canadian institutes for Health Research. J.B.C. is supported by the Huntington Society of Canada. M.R.H. is supported by the Canadian Institutes of Health Research, the Huntington Society of Canada, the Hereditary Disease Foundation and the Canadian Genetic Diseases Network. M.R.H. is a Killam University Professor and holds a Canada Research Chair in Human Genetics. The Mouse Imaging Centre (MICE) acknowledges funding from the Canada Foundation for Innovation and the Ontario Innovation Trust for providing facilities along with The Hospital for Sick Children. Operating funds from the Burroughs Wellcome Fund, the Canadian Institutes of Health Research, the National Cancer Institute of Canada – Terry Fox Program Projects, the National Institutes of Health and the Ontario Research and Development Challenge Fund are gratefully acknowledged. R.M.H. holds a Canada Research Chair in Imaging. The authors would like to express appreciation to Jean Paul Vonsattel and Elizabeth Aylward for their thoughtful suggestions.

## References

- Aylward, E.H., 2007. Change in MRI striatal volumes as a biomarker in preclinical Huntington's disease. *Brain Res Bull.* 72 (2–3), 152–158.
- Aylward, E.H., Anderson, N.B., Bylsma, F.W., Wagster, M.V., Barta, P.E., Sherr, M., Feeny, J., Davis, A., Rosenblatt, A., Pearlson, G.D., Ross, C.A., 1998. Frontal lobe volume in patients with Huntington's disease. *Neurology* 50 (1), 252–258.
- Aylward, E.H., Sparks, B.F., Field, K.M., Yallapragada, V., Shpritz, B.D., Rosenblatt, A., Brandt, J., Gourley, L.M., Liang, K., Zhou, H., Margolis, R.L., Ross, C.A., 2004. Onset and rate of striatal atrophy in preclinical Huntington disease. *Neurology* 63 (1), 66–72.
- Bock, N.A., Kovacevic, N., Lipina, T.V., Roder, J.C., Ackerman, S.L., Henkelman, R.M., 2006. *In vivo* magnetic resonance imaging and semiautomated image analysis extend the brain phenotype for *cdf/cdf* mice. *J. Neurosci.* 26 (17), 4455–4459.
- Chen, X.J., Kovacevic, N., Lobaugh, N.J., Sled, J.G., Henkelman, R.M., Henderson, J.T., 2006. Neuroanatomical differences between mouse strains as shown by high-resolution 3D MRI. *NeuroImage* 29 (1), 99–105.
- Chung, M.K., Worsley, K.J., Paus, T., Cherif, C., Collins, D.L., Giedd, J.N., Rapoport, J.L., Evans, A.C., 2001. A unified statistical approach to deformation-based morphometry. *NeuroImage* 14 (3), 595–606.

- Chung, M.K., Worsley, K.J., Robbins, S., Paus, T., Taylor, J., Giedd, J.N., Rapoport, J.L., Evans, A.C., 2003. Deformation-based surface morphometry applied to gray matter deformation. *NeuroImage* 18 (2), 198–213.
- Collins, D.L., Neelin, P., Peters, T.M., Evans, A.C., 1994. Automatic 3D intersubject registration of MR volumetric data in standardized Talairach space. *J. Comput. Assist. Tomogr.* 18 (2), 192–205.
- Collins, D.L., Holmes, C.J., Peters, T.M., Evans, A.C., 1995. Automatic 3D model-based neuroanatomical segmentation. *Hum. Brain Mapp.* 33, 190–208.
- Curtis, M.A., Penney, E.B., Pearson, A.G., van Roon-Mom, W.M., Butterworth, N.J., Dragunow, M., Connor, B., Faull, R.L., 2003. Increased cell proliferation and neurogenesis in the adult human Huntington's disease brain. *Proc. Natl. Acad. Sci. U. S. A.* 100 (15), 9023–9027.
- Curtis, M.A., Penney, E.B., Pearson, J., Dragunow, M., Connor, B., Faull, R.L., 2005. The distribution of progenitor cells in the subependymal layer of the lateral ventricle in the normal and Huntington's disease human brain. *Neuroscience* 132 (3), 777–788.
- Genovese, C.R., Lazar, N.A., Nichols, T., 2002. Thresholding of statistical maps in functional neuroimaging using the false discovery rate. *NeuroImage* 15 (4), 870–878.
- Hodgson, J.G., Agopyan, N., Gutekunst, C.A., Leavitt, B.R., LePiane, F., Singaraja, R., Smith, D.J., Bissada, N., McCutcheon, K., Nasir, J., Jamot, L., Li, X.J., Stevens, M.E., Rosemond, E., Roder, J.C., Phillips, A.G., Rubin, E.M., Hersch, S.M., Hayden, M.R., 1999. A YAC mouse model for Huntington's disease with full-length mutant *huntingtin*, cytoplasmic toxicity, and selective striatal neurodegeneration. *Neuron* 23 (1), 181–192.
- Huntington's Collaborative Research, G.r.o.u.p., 1993. A novel gene containing a trinucleotide repeat that is expanded and unstable on Huntington's disease chromosomes. The Huntington's Disease Collaborative Research Group. *Cell* 72 (6), 971–983.
- Jenkins, B.G., Rosas, H.D., Chen, Y.C., Makabe, T., Myers, R., MacDonald, M., Rosen, B.R., Beal, M.F., Koroshetz, W.J., 1998. <sup>1</sup>H NMR spectroscopy studies of Huntington's disease: correlations with CAG repeat numbers. *Neurology* 50 (5), 1357–1365.
- Kipps, C.M., Duggins, A.J., Mahant, N., Gomes, L., Ashburner, J., McCusker, E.A., 2005. Progression of structural neuropathology in preclinical Huntington's disease: a tensor based morphometry study. *J. Neurol. Neurosurg. Psychiatry* 76 (5), 650–655.
- Kovacevic, N., Henderson, J.T., Chan, E., Lifshitz, N., Bishop, J., Evans, A.C., Henkelman, R.M., Chen, X.J., 2005. A three-dimensional MRI atlas of the mouse brain with estimates of the average and variability. *Cereb. Cortex* 15 (5), 639–645.
- MacKenzie-Graham, A., Tinsley, M.R., Shah, K.P., Aguilar, C., Strickland, L.V., Boline, J., Martin, M., Morales, L., Shattuck, D.W., Jacobs, R.E., Voskuhl, R.R., Toga, A.W., 2006. Cerebellar cortical atrophy in experimental autoimmune encephalomyelitis. *NeuroImage* 32 (3), 1016–1023.
- Nieman, B.J., Bock, N.A., Bishop, J., Chen, X.J., Sled, J.G., Rossant, J., Henkelman, R.M., 2005. Magnetic resonance imaging for detection and analysis of mouse phenotypes. *NMR Biomed.* 18 (7), 447–468.
- Paulsen, J.S., Magnotta, V.A., Mikos, A.E., Paulson, H.L., Penziner, E., Andreasen, N.C., Nopoulos, P.C., 2006. Brain structure in preclinical Huntington's disease. *Biol. Psychiatry* 59 (1), 57–63.
- Rosas, H.D., Goodman, J., Chen, Y.I., Jenkins, B.G., Kennedy, D.N., Makris, N., Patti, M., Seidman, L.J., Beal, M.F., Koroshetz, W.J., 2001. Striatal volume loss in HD as measured by MRI and the influence of CAG repeat. *Neurology* 57 (6), 1025–1028.
- Rosas, H.D., Liu, A.K., Hersch, S., Glessner, M., Ferrante, R.J., Salat, D.H., van der Kouwe, A., Jenkins, B.G., Dale, A.M., Fischl, B., 2002. Regional and progressive thinning of the cortical ribbon in Huntington's disease. *Neurology* 58 (5), 695–701.
- Rosas, H.D., Koroshetz, W.J., Chen, Y.I., Skeuse, C., Vangel, M., Cudkovic, M.E., Caplan, K., Marek, K., Seidman, L.J., Makris, N., Jenkins, B.G., Goldstein, J.M., 2003. Evidence for more widespread cerebral pathology in early HD: an MRI-based morphometric analysis. *Neurology* 60 (10), 1615–1620.
- Slow, E.J., van Raamsdonk, J., Rogers, D., Coleman, S.H., Graham, R.K., Deng, Y., Oh, R., Bissada, N., Hossain, S.M., Yang, Y.Z., Li, X.J., Simpson, E.M., Gutekunst, C.A., Leavitt, B.R., Hayden, M.R., 2003. Selective striatal neuronal loss in a YAC128 mouse model of Huntington disease. *Hum. Mol. Genet.* 12 (13), 1555–1567.
- Spring, S., Lerch, J.P., Henkelman, R.M., 2007. Sexual dimorphism revealed in the structure of the mouse brain using three-dimensional magnetic resonance imaging. *NeuroImage* 35 (4), 1424–1433.
- Tattersfield, A.S., Croon, R.J., Liu, Y.W., Kells, A.P., Faull, R.L., Connor, B., 2004. Neurogenesis in the striatum of the quinolinic acid lesion model of Huntington's disease. *Neuroscience* 127 (2), 319–332.
- Tyszka, J.M., Readhead, C., Bearer, E.L., Pautler, R.G., Jacobs, R.E., 2006. Statistical diffusion tensor histology reveals regional dysmyelination effects in the *shiverer* mouse mutant. *NeuroImage* 29 (4), 1058–1065.
- Van Raamsdonk, J.M., Murphy, Z., Slow, E.J., Leavitt, B.R., Hayden, M.R., 2005a. Selective degeneration and nuclear localization of mutant *huntingtin* in the YAC128 mouse model of Huntington disease. *Hum. Mol. Genet.* 14 (24), 3823–3835.
- Van Raamsdonk, J.M., Pearson, J., Bailey, C.D., Rogers, D.A., Johnson, G.V., Hayden, M.R., Leavitt, B.R., 2005b. Cystamine treatment is neuroprotective in the YAC128 mouse model of Huntington disease. *J. Neurochem.* 95 (1), 210–220.
- Van Raamsdonk, J.M., Pearson, J., Rogers, D.A., Lu, G., Barakauskas, V.E., Barr, A.M., Honer, W.G., Hayden, M.R., Leavitt, B.R., 2005c. Ethyl-EPA treatment improves motor dysfunction, but not neurodegeneration in the YAC128 mouse model of Huntington disease. *Exp. Neurol.* 196 (2), 266–272.
- Van Raamsdonk, J.M., Pearson, J., Slow, E.J., Hossain, S.M., Leavitt, B.R., Hayden, M.R., 2005d. Cognitive dysfunction precedes neuropathology and motor abnormalities in the YAC128 mouse model of Huntington's disease. *J. Neurosci.* 25 (16), 4169–4180.
- Van Raamsdonk, J.M., Pearson, J., Murphy, Z., Hayden, M.R., Leavitt, B.R., 2006. Wild-type *huntingtin* ameliorates striatal neuronal atrophy but does not prevent other abnormalities in the YAC128 mouse model of Huntington disease. *BMC Neurosci.* 7, 80.
- Vonsattel, J.P., Myers, R.H., Stevens, T.J., Ferrante, R.J., Bird, E.D., Richardson Jr., E.P., 1985. Neuropathological classification of Huntington's disease. *J. Neuropathol. Exp. Neurol.* 44 (6), 559–577.